RAA 2015 Vol. **15** No. **6**, 785–801 doi: 10.1088/1674–4527/15/6/002
http://www.raa-journal.org *http://www.iop.org/journals/raa*

Research in Astronomy and Astrophysics

CO observations towards a sample of nearby galaxies

Fa-Cheng Li[1,2], Yuan-Wei Wu[1] and Ye Xu[1]

[1] Purple Mountain Observatory, & Key Laboratory for Radio Astronomy, Chinese Academy of Sciences, Nanjing 210008, China; *lifc@pmo.ac.cn*
[2] University of Chinese Academy of Sciences, Beijing 100049, China

Received 2013 November 26; accepted 2014 November 13

Abstract We have simultaneously observed ^{12}CO, ^{13}CO and C^{18}O ($J = 1 - 0$) rotational transitions in the centers of a sample of 58 nearby spiral galaxies using the 13.7-m millimeter-wave telescope administered by Purple Mountain Observatory. Forty-two galaxies were detected in ^{13}CO emission, but there was a null detection for C^{18}O emission with a σ upper limit of 2 mK. The central beam ratios, $\mathcal{R}$, of ^{12}CO and ^{13}CO range mostly from 5 to 13, with an average value of 8.1±4.2, which is slightly lower than previous estimates for normal galaxies. Clear correlations are found between ^{12}CO and ^{13}CO luminosities. An average X factor of $1.44 \pm 0.84 \times 10^{20}\ \mathrm{cm^{-2}\ (K\ km\ s^{-1})^{-1}}$ is slightly lower than that in the Milky Way.

Key words: galaxies: ISM — molecules: galaxies — millimeter lines: ISM — star formation: ISM

1 INTRODUCTION

Molecular hydrogen, H_2, constitutes a dominant part of molecular clouds in the interstellar medium in galaxies and is most closely related to star formation. The current method of studying molecular clouds in external galaxies involves the observation of rotational transitions of carbon monoxide, CO. H_2 lacks a dipole moment and therefore, quadrupole or vibrational transitions cannot be excited under typical cold temperature conditions that exist in giant molecular clouds. Rotational transitions of CO can easily be generated by collisions with H_2, particularly the line from the first excited level to ground, $J = 1 - 0$, which can be excited under the conditions of very low temperature and density of only 10 K and 300 cm^{-3} respectively. Thus, ^{12}CO, as well as its isotopic variants, remain the most straightforward and reliable tracer of H_2 in molecular clouds. In addition, there is a well-known CO$-$H$_2$ conversion factor, called the X factor, and it is defined as

$$X_{\rm CO} = \frac{N({\rm H_2})}{I_{\rm CO}} \left[{\rm cm^{-2}\ (K\ km\ s^{-1})^{-1}}\right], \quad (1)$$

where $N(\mathrm{H_2})$ is the column density of H_2 in cm^{-2} and $I_{\rm CO}$ is the integrated line intensity of ^{12}CO.

The first CO detections in external galaxies were carried out by Rickard et al. (1975) and Solomon & de Zafra (1975). Later, Young et al. (1995) published the Five College Radio Astronomy Observatory (FCRAO) Extragalactic CO Survey at $\lambda = 2.6$ mm of a large sample of 300 galaxies with 1412 positions using the 14 m telescope that has a 45$''$ resolution. The detection rate is 79% and 193 galaxies were observed in multiple positions. Braine et al. (1993) observed both

^{12}CO(1−0) and ^{12}CO(2−1) emission from the centers of 81 nearby spiral galaxies using the 30-m telescope at the Institut de Radioastronomie Millimétrique (IRAM) at a resolution of 23″ and 12″ for ^{12}CO(1−0) and ^{12}CO(2−1), respectively, and found the average (and median) ^{12}CO(2−1) to ^{12}CO(1−0) line ratio to be 0.89±0.06. Solomon et al. (1997) also used the IRAM 30-m telescope to observe ^{12}CO(1−0) transitions in 37 ultraluminous infrared galaxies and discovered that interacting galaxies also have relatively high CO luminosity. There are plenty of other CO surveys of nearby galaxies using either single-dishes or even interferometer telescopes that have aimed to map the molecular gas distribution or kinematics within galaxies and have been used to work out properties of molecular gas clouds from galaxy to galaxy (Sakamoto et al. 1999; Nishiyama et al. 2001; Helfer et al. 2003; Leroy et al. 2009). However, most of these surveys were based on ^{12}CO $J = 1 - 0$, $J = 2 - 1$ or even higher rotational transitions, and there are a few systematic studies of transitions in CO isotopes from a larger sample of galaxies that have been published. This is probably because ^{12}CO ($J = 1 - 0$) is not found to be an accurate measure of the amount of molecular gas, but ^{13}CO emission in conditions with lower opacity may give more reliable constraints on the H_2 column density.

Sage & Isbell (1991) presented observations of ^{13}CO (1−0) emission from 16 nearby spiral galaxies using the 12-m telescope at the National Radio Astronomy Observatory. They found the ratio of ^{12}CO (1−0) to ^{13}CO (1−0) emittance to be insensitive to variations in global parameters such as inclination angle and Hubble type. The detection revealed a range of central beam ratios from 5 to 16.6, mostly from 7 to 11. Aalto et al. (1995) studied molecular gas in 32 infrared-bright galaxies, which consists mostly of starbursts. They presented several line ratios, among which they suggested that the ratio of ^{12}CO/^{13}CO (1−0) can be a measurement of the cloud environment in galaxies. Paglione et al. (2001) performed a mapping survey of ^{12}CO and ^{13}CO ($J = 1 - 0$) emissions along the major axes of 17 nearby galaxies. Their work resulted in an average central ^{12}CO/^{13}CO intensity ratio of 11.6±1.9, implying that the X factor is probably lower in most galactic nuclei. A nonlinear correlation between CO and far-infrared luminosity exists in galaxies because luminous galaxies have a higher star formation efficiency (Solomon & Sage 1988; Young & Scoville 1991; Gao & Solomon 2004). Taniguchi & Ohyama (1998) collected previous observational results of ^{12}CO and ^{13}CO emissions and compared far-infrared luminosity with that of ^{12}CO and ^{13}CO, respectively. They found that the ^{13}CO depression in luminous starburst mergers may account for a higher abundance ratio of ^{12}CO to ^{13}CO than that in normal galaxies. Solomon & Vanden Bout (2005) and Daddi et al. (2010) further confirmed the validity of this correlation when studying high-redshift star forming galaxies.

In order to systemically study the physical properties of external galaxies, we present simultaneous observations of ^{12}CO, ^{13}CO and C^{18}O ($J = 1 - 0$) emissions from the centers of 58 nearby galaxies, mostly spiral, using the 13.7-m millimeter radio telescope administered by Purple Mountain Observatory (PMO). This is the second time we have carried out observations towards nearby galaxies using this telescope after Tan et al. (2011). The observations and sample selection are described in Section 2. We then present the results with detected CO spectra and derived parameters in Section 3. The analysis and discussions are described in Section 4 and finally the summary is given in Section 5.

2 SAMPLE AND OBSERVATIONS

2.1 Sample Selection

We selected a sample of 58 nearby galaxies from the FCRAO Extragalactic CO Survey (Young et al. 1995). The selection criteria were as follows: (1) $I(^{12}\mathrm{CO}) \geq 3$ K km s^{-1}, where K is the antenna temperature. Strong ^{12}CO emission usually indicates a relatively high detection rate of isotopic variants. (2) Coordinates in the range $10\mathrm{h} \leq \mathrm{R.A.} \leq 13\mathrm{h}$ and Dec. $\geq -10°$, in order to not conflict with the time observing the Galactic plane in the northern sky. The physical properties of the galaxies, as derived from data taken with the Infrared Astronomical Satellite (IRAS), are summarized in Table 1. These values were obtained from the IRAS Revised Bright Galaxy Sample (RBGS) (Sanders et al. 2003) and the SIMBAD database.

Table 1 Basic Properties of the Sample

Galaxy Name	Type	R.A. Dec. (J2000)	cz (km s^{-1})	D (Mpc)	IR size major×minor (arcmin)	$T_{\rm dust}$ (K)
(1)	(2)	(3)	(4)	(5)	(6) (7)	(8)
M66	Sb	11:20:15.026 +12:59:28.64	740	10.04	6.64×3.65	34.71
M108	Sc	11:11:30.967 +55:40:26.84	698	13.85	7.91×1.74	33.07
NGC 3079	S	10:01:57.924 +55:40:48.00	1142	18.19	4.49×1.08	34.67
NGC 3169	Sb	10:14:15.099 +03:27:58.03	1305	20.61	2.73×2.02	31.24
NGC 3184	Sc	10:18:16.985 +41:25:27.77	593	12.58	6.72×5.72	29.71
NGC 3593	S0	11:14:37.002 +12:49:04.87	578	5.04	3.48×1.43	35.25
NGC 3628	Sbc	11:20:17.018 +13:35:22.16	825	10.04	10.58×2.54	35.54
NGC 3631	Sc	11:21:02.944 +53:10:09.95	1158	21.58	4.19×4.02	31.07
NGC 3672	Sc	11:25:02.476 −09:47:43.44	1899	27.70	2.97×1.13	31.30
NGC 3675	Sb	11:26:08.584 +43:35:09.30	804	12.69	4.45×2.00	29.15
NGC 3690	Sm	11:28:31.600 +58:33:44.00	3159	47.74	1.61×1.41	47.31
NGC 3810	Sc	11:40:58.737 +11:28:16.07	1001	15.36	3.05×2.08	32.12
NGC 3893	Sc	11:48:38.207 +48:42:38.84	892	16.35	2.88×2.13	33.06
NGC 3938	Sc	11:52:49.453 +44:07:14.63	800	14.75	4.00×3.80	30.57
NGC 4030	Scdr	12:00:23.643 −01:05:59.87	1427	24.50	2.67×2.35	31.41
NGC 4038	Sc	12:01:52.480 −18:52:02.90	1563	21.54	5.20×3.10	35.55
NGC 4039	Sc	12:01:53.700 −18:53:08.00	1563	21.54	3.10×1.60	35.55
NGC 4041	Sc	12:02:12.173 +62:08:14.23	1243	22.78	1.70×1.39	33.67
NGC 4051	SBab	12:03:09.686 +44:31:52.54	728	13.11	4.73×2.60	33.04
NGC 4088	Sc	12:05:34.189 +50:32:20.50	696	13.37	4.39×2.11	33.35
NGC 4096	Sc	12:06:01.161 +47:28:42.09	523	9.63	5.76×1.73	30.21
NGC 4102	Sb	12:06:23.115 +52:42:39.42	859	16.89	1.78×0.98	39.20
NGC 4157	Sb	12:11:04.365 +50:29:04.85	790	13.30	4.94×0.89	31.02
NGC 4194	I	12:14:09.573 +54:31:36.03	2555	40.33	0.67×0.46	45.18
NGC 4212	Sc	12:15:39.375 +13:54:05.30	−81	15.29	2.97×1.42	32.15
NGC 4254	Sc	12:18:49.625 +14:24:59.36	2403	15.29	4.50×4.27	32.65
NGC 4258	Sbc	12:18:57.620 +47:18:13.39	448	7.10	11.14×5.46	-
NGC 4273	SBc	12:19:56.063 +05:20:36.12	2400	15.29	1.71×1.20	33.27
NGC 4293	Sap	12:21:12.891 +18:22:56.64	893	16.50	5.29×1.80	-
NGC 4298	Sc	12:21:32.790 +14:36:21.78	1141	15.29	2.97×1.78	28.71
NGC 4302	Sc	12:21:42.477 +14:35:51.94	1149	19.20	5.37×0.64	-
NGC 4303	SABbc	12:21:54.950 +04:28:24.92	1570	15.29	4.64×3.48	34.39
NGC 4312	Sa	12:22:31.359 +15:32:16.51	153	16.50	3.39×0.88	30.75
NGC 4321	Sc	12:22:54.899 +15:49:20.57	1571	15.20	7.23×5.64	31.89
NGC 4402	Sb	12:26:07.566 +13:06:46.06	237	15.29	2.97×0.59	30.04
NGC 4414	Sc	12:26:27.089 +31:13:24.76	720	17.68	2.86×1.60	32.92
NGC 4419	SBa	12:26:56.433 +15:02:50.72	−261	15.29	2.54×0.81	34.26
NGC 4433	Sbc	12:27:38.610 −08:16:42.42	2913	41.68	1.52×0.55	36.60
NGC 4457	SB0/Sa	12:28:59.011 +03:34:14.19	882	12.40	2.00×1.36	34.84
NGC 4490	Sd	12:30:36.710 +41:38:26.60	641	10.48	5.32×2.29	35.83
NGC 4501	Sbc	12:31:59.216 +14:25:13.48	2284	15.29	5.47×2.41	29.94
NGC 4527	Sb	12:34:08.496 +02:39:13.72	1771	15.29	4.62×1.57	34.51
NGC 4535	SBc	12:34:20.310 +08:11:51.94	1957	15.77	5.84×2.92	31.09
NGC 4536	Sc	12:34:27.129 +02:11:16.37	1802	14.92	4.61×2.40	39.51
NGC 4567	Sc	12:36:32.703 +11:15:28.33	2262	15.29	3.72×2.19	31.50
NGC 4568	Sc	12:36:34.292 +11:14:19.07	2262	15.29	4.06×1.59	31.50

Table 1 — *Continued.*

Galaxy Name	Type	R.A. Dec. (J2000)	cz (km s^{-1})	D (Mpc)	IR size major×minor (arcmin)		$T_{\rm dust}$ (K)
(1)	(2)	(3)	(4)	(5)	(6)	(7)	(8)
NGC 4569	Sab	12:36:49.816 +13:09:46.33	−235	15.29	6.92×2.77		31.57
NGC 4579	Sab	12:37:43.527 +11:49:05.46	1519	7.73	4.60×3.22		28.86
NGC 4631	Sc	12:42:08.009 +32:32:29.44	630	15.29	9.25×2.78		35.93
NGC 4647	Sc	12:43:32.542 +11:34:56.89	1415	15.29	2.58×2.04		30.97
NGC 4654	SBcd	12:43:56.638 +13:07:34.86	1037	12.82	4.47×2.01		31.16
NGC 4666	Sbc	12:45:08.676 −00:27:42.88	1495	20.65	3.32×0.93		33.29
NGC 4691	S0a	12:48:13.600 −03:19:57.70	1124	21.71	2.80×2.30		38.37
NGC 4710	S0a	12:49:38.958 +15:09:55.76	1125	15.29	3.73×0.90		33.67
NGC 4736	Sb	12:50:53.148 +41:07:12.55	323	4.83	4.13×3.27		37.40
NGC 4818	Sab	12:56:48.907 −08:31:31.08	1051	9.37	3.34×1.60		41.33
NGC 4826	Sb	12:56:43.696 +21:40:57.57	349	3.09	6.82×3.89		33.76
NGC 4845	Sb	12:58:01.242 +01:34:32.09	1224	15.09	3.85×1.08		32.93

Column (1): Names of the sample galaxies. Column (2): Morphological types taken from the SIMBAD database (*http://simbad.u-strasbg.fr/simbad/*). Column (3): Adopted tracking center of observed galaxies; units of right ascension are hours, minutes and seconds, and units of declination are degrees, arcminutes and arcseconds. The data in Columns (4)–(5) except for NGC 4258, NGC 4293, NGC 4302, NGC 4312 and NGC 4457 are taken from Sanders et al. (2003). Column (4): The heliocentric radial velocity computed as c times the redshift z. Column (5): Distances including luminosity distance and distance measured in other ways. Columns (6)–(7): Infrared angular sizes mostly taken from 2MASS data using SIMBAD. Column (8): Dust temperature derived from the RBGS IRAS 60 μm/100 μm color assuming an emissivity that is proportional to the frequency ν; those without RBGS (Sanders et al. 2003) data are calculated following Sanders & Mirabel (1996) using the *IRAS Point Source Catalog* (PSC:1988).

2.2 Observations

We made observations between February and June 2011 and supplementary observations between September and October 2011 and also December 2012, using the PMO 13.7-m millimeter-wave telescope located at Delingha, Qinghai, China. The observations were made after the newly developed 3×3 multi-beam sideband separation superconducting spectroscopic array receiver (SSAR) was added. The receiver employs a two-sideband superconductor-insulator-superconductor (SIS) mixer, which allowed us to simultaneously observe ^{12}CO $(J = 1 - 0)$ emission in the upper sideband (USB) and ^{13}CO and C^{18}O $(J = 1 - 0)$ emissions in the lower sideband (LSB). A high definition Fast Fourier Transform Spectrometer as the backend enabled a bandwidth of 1 GHz and a velocity resolution of 0.16 km s^{-1} at 115.271 GHz. Single-point observations using beam 5 of SSAR were done in the "On-Off" position switching mode, with a pointing accuracy of nearly 5″. The Half Power Beam Width was 52″ at 115.271 GHz and the main beam efficiency, $\eta_{\rm mb}$, for USB and LSB were 0.46 and 0.5 respectively between February and June 2011 and were 0.44 and 0.48 during October 2011[1]. Typical system temperatures were 220 K at 115.271 GHz and 130 K at 110.201 GHz during our observations.

3 RESULTS

3.1 Data Reduction

We reduced the data using CLASS, which is a part of the GILDAS[2] software package. The original data included individual scans. For each spectrum, line-free channels that exhibited positive or neg-

[1] See the Status Report *http://www.radioast.csdb.cn/zhuangtaibaogao.php*
[2] *http://www.iram.fr/IRAMFR/GILDAS/*

ative spikes more than 5σ above the rms noise were blanked or substituted with values interpolated from adjacent ones. This was only done after properly setting the velocity range limits for each spectrum and a linear baseline was subtracted from it. We then examined every spectrum and identified those with a relatively bad baseline and an abnormally high rms noise. Due to unstable spectrum baselines and bad weather conditions, a considerable part of the data was discarded. After converting the temperature scale to $T_{\rm mb}$ from $T_{\rm A}^*$ of the spectra and dividing by $\eta_{\rm mb}$, we then averaged the converted data, weighting by the inverse square of the rms noise, σ. Note however that data from different observational seasons were treated differently. The final averaged spectra of each source were smoothed to a velocity resolution of about 20 km s^{-1} for ^{12}CO and about 40 km s^{-1} for ^{13}CO in order to limit the rms noise. Each averaged spectrum was fitted using the GAUSS method and the results are presented in the next subsection.

3.2 Observational Results

We simultaneously observed ^{12}CO, ^{13}CO and C^{18}O emissions at the centers of 58 nearby galaxies, among which 42 had detections of ^{13}CO emission with a signal-to-noise ratio of more than 3. However, C^{18}O emission was too weak to be detected in any galaxy with an upper limit of 2 mK (1σ). Both ^{12}CO and ^{13}CO line profiles agree very well with similar centroid velocities and line widths in most cases, as shown in Figure 1. All of the spectra were smoothed to a velocity resolution of about 20 km s^{-1} for ^{12}CO and about 40 km s^{-1} for ^{13}CO to improve the signal-to-noise ratio. These values are given in Table 2. We do not show those ^{12}CO spectra without ^{13}CO detection since one can easily find them in the literature.

The integrated intensity, $I_{\rm CO}$, can be obtained by integrating $T_{\rm mb}$ over the line emission feature,

$$I_{\rm CO} \equiv \int T_{\rm mb} dv \; [\rm K\ km\ s^{-1}] \,, \tag{2}$$

and the error of the integrated intensity is estimated through the following formula (Elfhag et al. 1996),

$$\delta I = \sigma_{\rm rms} \sqrt{\frac{\Delta v dV}{(1-\Delta v/W)}} \; [\rm K\ km\ s^{-1}] \,, \tag{3}$$

where $\sigma_{\rm rms}$ is the rms noise temperature, Δv is the line width of the emission feature, dV is the spectrum velocity resolution, and W is the entire velocity range of each spectrum. These properties for each spectrum are presented in Figure 1: W is taken from the visible velocity range in each plot; Δv is the window for the emission feature drawn on the bottom; dV is labeled. For those without detection of ^{13}CO, $2\delta I_{13}$ upper limits were given based on estimates by using the expected line width from the detected ^{12}CO lines at exactly the same position. The peak velocities and line widths come from a Gaussian fit. The ratio of ^{12}CO and ^{13}CO integrated intensity is defined as

$$\mathcal{R} \equiv \frac{\int T_{\rm mb}(^{12}{\rm CO}) dv}{\int T_{\rm mb}(^{13}{\rm CO}) dv} \,. \tag{4}$$

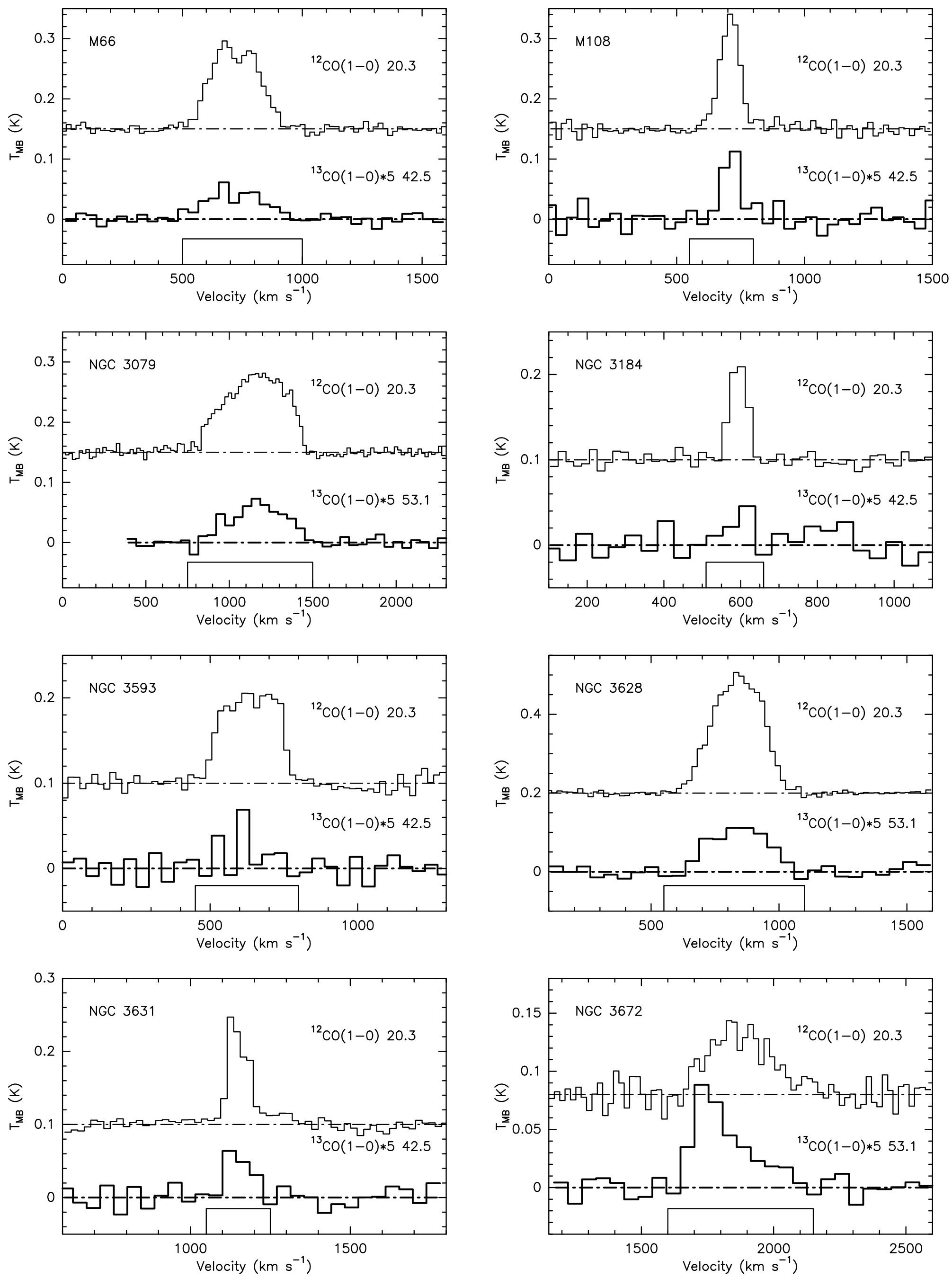

Fig. 1 Observed spectra of ^{12}CO (*thin lines*) and ^{13}CO (*thick lines*) in the central regions of galaxies where ^{13}CO was detected. Velocities are the radio velocities with respect to LSR. The spectra of ^{13}CO emissions are multiplied by 5 for comparison. The spectra are on the scale of main beam temperature. All the spectra were smoothed to a velocity resolution of about 20 km s^{-1} for ^{12}CO and about 40 km s^{-1} for ^{13}CO in order to limit the rms noise. The number to the right of the spectrum label is the specified velocity resolution for the individual source. The window for the emission feature is drawn as a box on the bottom of the axis in each plot.

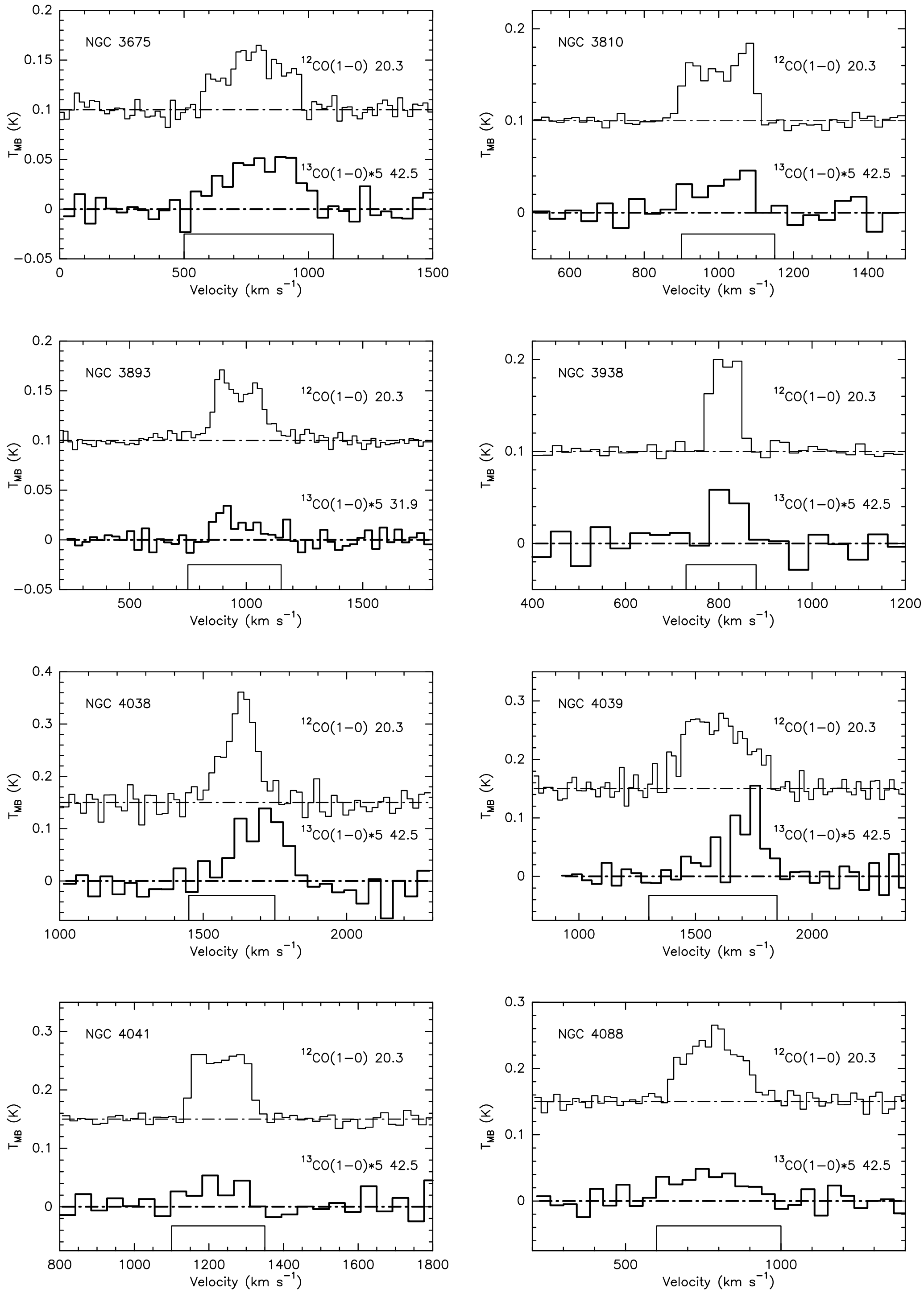

Fig. 1 – *Continued.*

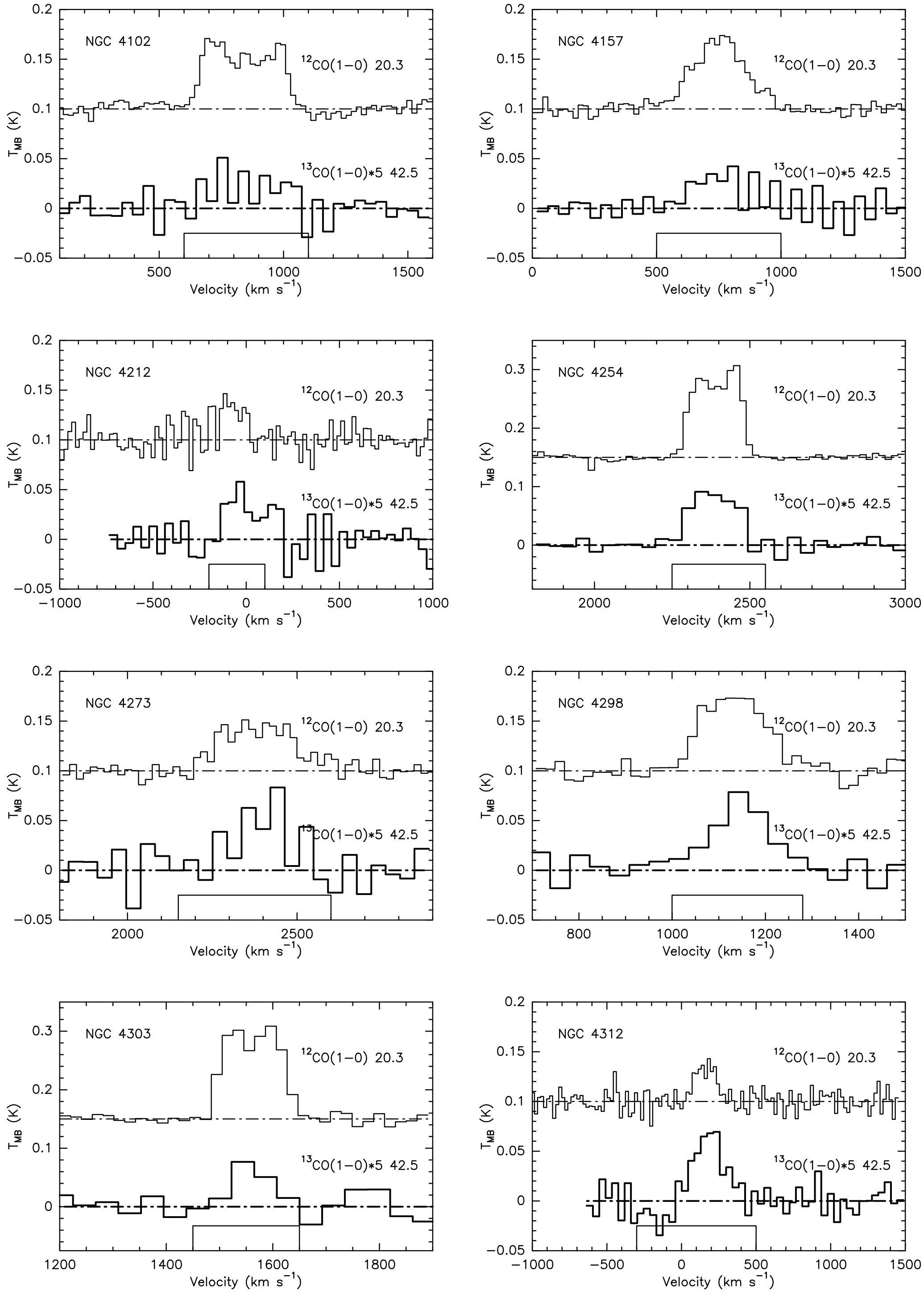

Fig. 1 – *Continued.*

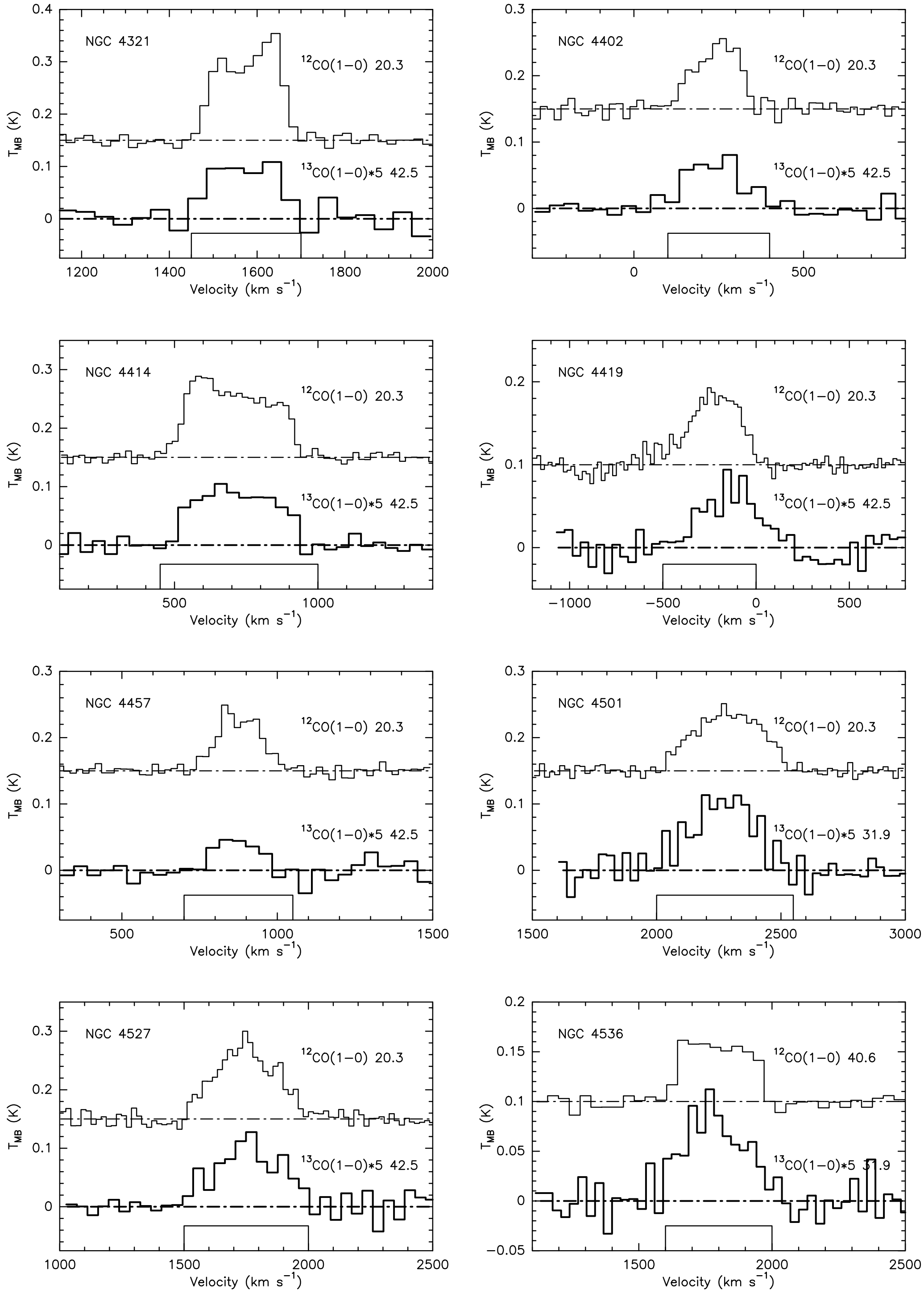

Fig. 1 *– Continued.*

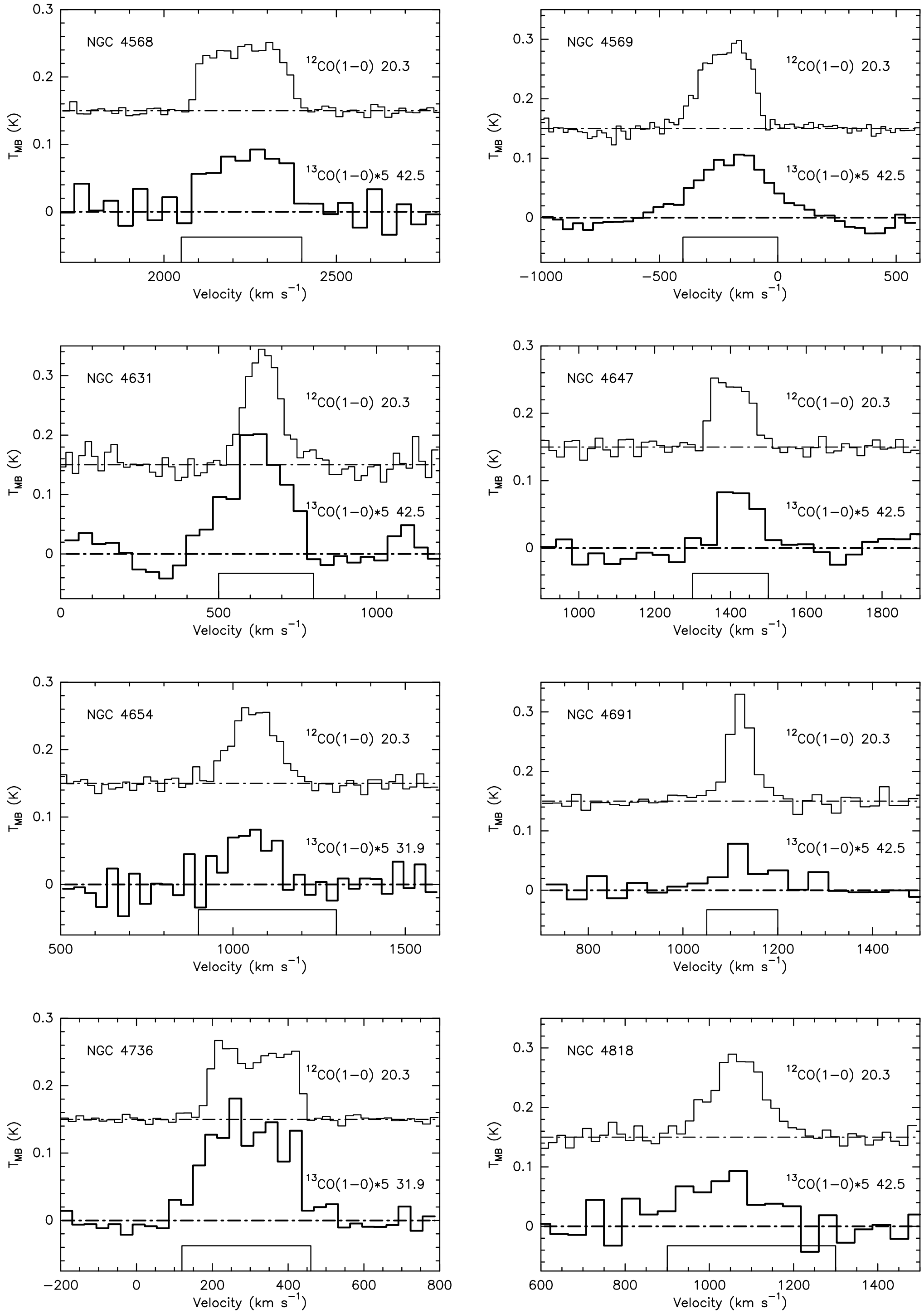

Fig. 1 – *Continued.*

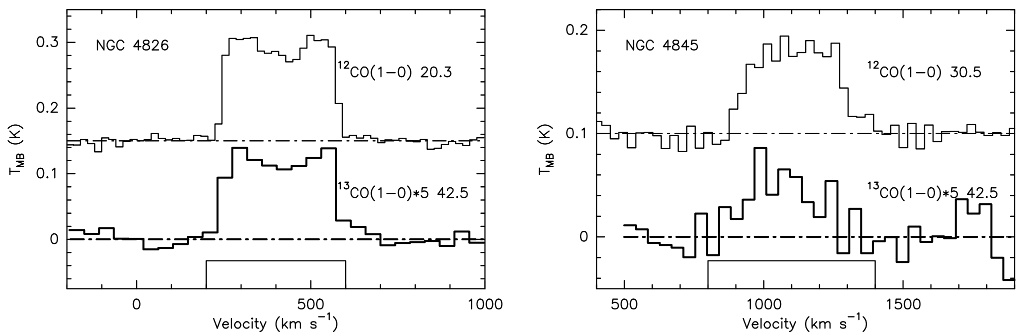

Fig. 1 – *Continued.*

Table 2 Observational Results

Galaxy	^{12}CO(1−0)				^{13}CO(1−0)				$\mathcal{R}$
	$I \pm \delta I$ (K km s^{-1})	$\sigma_{\rm rms}$ (mK)	V (km s^{-1})	ΔV	$I \pm \delta I$ (K km s^{-1})	$\sigma_{\rm rms}$ (mK)	V (km s^{-1})	ΔV	
(1)	(2)	(3)	(4)	(5)	(6)	(7)	(8)	(9)	(10)
M66	33.89±0.67	5.54	719	233	2.75±0.22	1.28	714	283	12.32±1.02
M108	17.94±0.67	8.58	708	89	2.01±0.37	3.29	713	73	8.93±1.68
NGC 3079	59.17±0.96	6.38	1160	425	5.11±0.28	1.17	1176	378	11.58±0.66
NGC 3169	31.66±1.33	7.69	1182	447	<1.50	2.46	–	–	>21.11
NGC 3184	6.52±0.44	7.42	594	52	0.56±0.25	2.89	601	42	11.64±5.26
NGC 3593	24.34±0.78	7.86	637	212	1.02±0.34	2.37	616	42	23.86±7.99
NGC 3628	72.66±0.59	4.44	840	226	5.92±0.59	2.73	843	252	12.27±1.23
NGC 3631	11.29±0.51	7.33	1147	76	1.17±0.27	2.66	1146	91	9.65±2.27
NGC 3672	15.58±1.31	9.76	1870	265	3.55±0.33	1.53	1769	186	4.39±0.55
NGC 3675	17.13±1.05	7.37	786	282	3.26±0.42	2.04	814	312	5.25±0.75
NGC 3690	24.29±0.66	4.87	3093	260	<0.46	1.36	–	–	>52.80
NGC 3810	12.42±0.47	5.07	1006	183	1.39±0.27	2.03	1016	181	8.94±1.77
NGC 3893	13.63±0.53	5.08	963	238	0.83±0.20	1.51	927	153	16.42±4.01
NGC 3938	7.47±0.33	5.42	813	66	0.85±0.23	2.56	820	42	8.79±2.41
NGC 4030	21.95±1.74	14.29	1454	290	<2.24	6.35	–	–	>9.80
NGC 4038	28.62±2.00	18.49	1632	127	5.74±0.76	4.83	1701	189	4.99±0.75
NGC 4039	39.93±1.96	14.06	1584	313	4.47±0.69	3.40	1734	146	8.93±1.45
NGC 4041	18.33±0.65	7.86	1234	152	1.39±0.46	3.84	1218	146	13.19±4.39
NGC 4051	10.66±0.53	4.71	705	141	<1.02	3.65	–	–	>10.45
NGC 4088	21.90±1.07	9.73	782	208	2.32±0.46	2.89	758	263	9.44±1.93
NGC 4096	6.58±0.72	6.40	546	136	<0.60	1.83	–	–	>10.97
NGC 4102	21.03±0.68	5.51	825	335	1.63±0.39	2.16	834	310	12.90±3.12
NGC 4157	17.88±0.61	4.94	751	241	1.93±0.44	2.44	764	300	9.26±2.14
NGC 4194	4.02±1.02	7.98	2515	139	<1.36	3.66	–	–	>2.96
NGC 4212	5.27±1.55	11.72	−85	156	1.45±0.59	3.09	−13	218	3.63±1.82
NGC 4254	25.55±0.49	5.44	2393	168	3.20±0.24	1.82	2380	164	7.98±0.62
NGC 4258	52.70±1.27	8.80	423	348	<2.46	6.80	–	–	>21.42
NGC 4273	11.77±0.81	6.52	2385	245	2.36±0.59	3.29	2405	178	4.99±1.29
NGC 4293	12.18±0.70	8.47	929	171	<0.54	2.24	–	–	>22.56
NGC 4298	12.69±0.72	7.74	1132	157	2.17±0.30	2.22	1148	137	5.85±0.87
NGC 4302	13.25±1.67	18.48	1134	190	<1.28	4.87	–	–	>10.35
NGC 4303	19.28±0.49	6.44	1563	118	1.31±0.41	3.72	1557	73	14.72±4.62
NGC 4312	5.93±1.46	9.46	162	160	2.57±0.58	2.58	184	224	2.31±0.77
NGC 4321	30.07±0.78	8.07	1585	162	3.60±0.56	3.98	1572	168	8.35±1.32
NGC 4402	15.82±0.85	9.24	247	153	2.79±0.37	2.82	235	194	5.67±0.81
NGC 4414	44.11±0.90	6.45	692	336	6.55±0.40	2.01	708	315	6.73±0.43
NGC 4419	26.82±1.41	9.50	−219	308	5.78±0.66	3.07	−135	333	4.64±0.58

Table 2 — *Continued.*

Galaxy	^{12}CO(1−0) $I \pm \delta I$ (K km s^{-1})	$\sigma_{\rm rms}$ (mK)	V (km s^{-1})	ΔV (km s^{-1})	^{13}CO(1−0) $I \pm \delta I$ (K km s^{-1})	$\sigma_{\rm rms}$ (mK)	V (km s^{-1})	ΔV (km s^{-1})	$\mathcal{R}$
(1)	(2)	(3)	(4)	(5)	(6)	(7)	(8)	(9)	(10)
NGC 4433	20.60±1.01	7.40	2946	273	<1.08	2.74	–	–	>19.07
NGC 4457	14.51±0.62	6.23	875	164	1.52±0.41	2.81	864	148	9.55±2.61
NGC 4490	3.18±0.43	6.02	609	125	<0.72	3.47	–	–	>4.42
NGC 4501	29.66±0.91	6.86	2288	315	6.58±0.59	3.56	2268	294	4.51±0.43
NGC 4527	37.20±1.21	9.80	1749	286	6.90±0.61	3.44	1759	311	5.39±0.51
NGC 4535	21.87±1.23	10.60	1993	199	<2.28	6.76	–	–	>9.59
NGC 4536	17.33±1.13	5.88	1786	274	4.81±0.56	3.32	1776	271	3.60±0.48
NGC 4567	12.33±0.47	5.58	2273	167	<0.58	2.39	–	–	>12.92
NGC 4568	24.46±0.61	5.97	2236	230	4.33±0.68	4.61	2247	238	5.65±0.90
NGC 4569	36.23±1.20	8.61	−214	234	7.92±0.48	2.39	−186	346	4.57±0.32
NGC 4579	11.38±1.08	9.81	1492	272	<1.30	4.09	–	–	>8.71
NGC 4631	11.73±0.74	9.00	639	125	2.18±0.41	3.45	622	199	5.38±1.07
NGC 4647	26.42±1.87	18.63	1401	111	8.36±0.72	4.96	1422	108	3.16±0.35
NGC 4654	16.81±0.97	8.54	1061	147	2.12±0.68	4.81	1051	146	7.93±2.58
NGC 4666	35.61±1.16	8.58	1525	268	<3.16	8.06	–	–	>11.26
NGC 4691	10.82±0.58	9.51	1122	56	1.08±0.31	3.50	1122	97	10.02±2.93
NGC 4710	14.97±1.03	7.43	1086	290	<1.06	2.61	–	–	>14.12
NGC 4736	24.31±0.43	4.16	308	224	7.38±0.38	2.95	293	240	3.29±0.18
NGC 4818	21.54±1.41	11.63	1067	146	3.21±0.91	5.21	1021	232	6.71±1.95
NGC 4826	48.17±0.65	5.88	409	298	8.40±0.33	2.08	413	306	5.73±0.24
NGC 4845	30.70±1.52	8.69	1118	320	3.55±0.77	3.74	1054	274	8.65±1.92

Column (1): Names of the sample galaxies. Column (2): ^{12}CO integrated intensities and uncertainties, calculated from Equation (2) and Equation (3). Column (3): Baseline noise of spectra in mK. Columns (4) and (5): Gaussian fitting results of peak velocities and FWHM line widths. Columns (6)−(9): Results for ^{13}CO, for non-detections, 2σ upper limits are given. Column (10): The ratios of ^{12}CO and ^{13}CO integrated intensities and their uncertainties.

3.3 Derived Properties

The derived physical parameters, such as the H_2 column density, the CO luminosity, and the gas mass, are presented in Table 3. We assumed that CO and its isotopic variants are approximately under the conditions of local thermodynamic equilibrium (LTE) when transitions occur and CO transitions are optically thick. Therefore we estimated the average optical depth of ^{13}CO from (Sage & Isbell 1991)

$$\tau^{13} \simeq -\ln\left[1 - \frac{\int T_{\rm R}^*(^{13}{\rm CO})dv}{\int T_{\rm R}^*(^{12}{\rm CO})dv}\right], \tag{5}$$

where $T_{\rm R}^*$ should be corrected for a filling factor and therefore this is only an averaged estimation over all of the unresolved clouds in the beam.

Due to the effect of beam dilution from molecular clouds in remote galaxies, we could not quite directly measure the excitation temperature, $T_{\rm ex}$. We present the cold dust color temperature, $T_{\rm dust}$, calculated from IRAS far infrared data assuming a dust emissivity, $\propto \nu^1$, in Table 1. However, the gas and dust in the central regions of the galaxies may not couple, and therefore, we took half the value of $T_{\rm dust}$ as the gas kinetic temperature as well as the excitation temperature, $T_{\rm ex} = T_{\rm k}$.

The H_2 column density of galaxies was estimated from an empirical equation (Nishiyama et al. 2001) in the Milky Way,

$$N({\rm H_2}) = 2 \times 10^{20} \int T_{\rm mb}(^{12}{\rm CO})dv\ [{\rm cm^{-2}}], \tag{6}$$

where the coefficient is the standard galactic ^{12}CO to H_2 conversion factor, X.

Using the LTE assumption, the total column density of the ^{13}CO (1-0) transition is described as (Wilson et al. 2009)

$$N(^{13}\mathrm{CO}) = 3.0 \times 10^{14} \frac{T_{\mathrm{ex}} \int \tau_{13} dv}{1 - \exp[-5.3/T_{\mathrm{ex}}]}\ [\mathrm{cm}^{-2}]\,. \tag{7}$$

Here, we assumed a filling factor of 1 and that ^{13}CO is optically thin so that there would be $T_{\mathrm{ex}}\ \tau = T_{\mathrm{mb}}$ and $T_{\mathrm{ex}} \int \tau_{13} dv = T_{\mathrm{mb}} \tau_{13}/(1 - \mathrm{e}^{-\tau_{13}})$. We then took a relatively high ratio of $N(\mathrm{H_2})/N(^{13}\mathrm{CO}) \sim 7.5 \times 10^5$ determined by the relationship between $N(^{13}\mathrm{CO})$ and visual extinction as well as $N(\mathrm{H_2})$ and A_{V}. Consequently, we also obtained the H_2 column density from the following equation,

$$N(\mathrm{H_2})' = 7.5 \times N(^{13}\mathrm{CO}) = 2.25 \times 10^{20} \frac{\tau_{13}}{1 - \mathrm{e}^{-\tau_{13}}} \frac{\int T_{\mathrm{mb}}(^{13}\mathrm{CO}) dv}{1 - \exp[-5.3/T_{\mathrm{ex}}]}\ [\mathrm{cm}^{-2}]\,. \tag{8}$$

By equating the H_2 column density derived both from ^{12}CO and ^{13}CO, we can estimate the kinetic temperature as well as the excitation temperature of the molecular gas in each galaxy.

The CO luminosity in $\mathrm{K\ km\ s^{-1}\ pc^2}$ can be defined as (Taniguchi & Ohyama 1998)

$$L_{\mathrm{CO}} \equiv \mathrm{area} \times I(\mathrm{CO}) = \frac{\pi \theta_{\mathrm{mb}}^2 D^2}{4 \ln 2} \int T_{\mathrm{mb}} dv\ [\mathrm{K\ km\ s^{-1}\ pc^2}]\,, \tag{9}$$

where $\pi \theta_{\mathrm{mb}}^2 D^2 / 4 \ln 2$ is the total area of a Gaussian beam source in units of pc^2 and θ_{mb} is the size of the beam in arcseconds. Furthermore, the CO luminosity can be equivalently expressed for a source of any size in terms of the total line flux (Solomon et al. 1997),

$$L_{\mathrm{CO}} = \frac{c^2}{2k} S(\mathrm{CO}) \nu_{\mathrm{obs}}^{-2} D^2 (1+z)^{-3} = 3.25 \times 10^7 S(\mathrm{CO}) \nu_{\mathrm{obs}}^{-2} D^2 (1+z)^{-3}\,. \tag{10}$$

Here L_{CO} is in $\mathrm{K\ km\ s^{-1}\ pc^2}$, k is the Boltzmann constant, ν_{obs} is the observational frequency we received, and

$$S(\mathrm{CO}) = \frac{2k\Omega \int T_{\mathrm{mb}} dv}{\lambda^2} \tag{11}$$

is the flux of CO in Jy, where Ω is the solid angle of the source beam.

Taking the H_2 column density derived from the ^{13}CO emission, we can calibrate the X factor.

4 DISCUSSION

We confirmed the detection of ^{13}CO emissions in 42 galaxies. However, this does not mean that other galaxies do not have ^{13}CO emissions. The limitation on detection caused by a wavelike baseline reaches beyond the signal of those with relatively weak sources. Among these weak sources, both ^{12}CO and ^{13}CO were detected in 42 cases. We present the central intensity ratio, $\mathcal{R}$, with an average value of 8.14±4.21, ranging mostly from 5 to 13. NGC 4212, NGC 4312, NGC 4536, NGC 4631 and NGC 4736 have very low ratios of less than 4. This is probably due to systematic uncertainties or a higher optical depth of the gas in the central positions of the galaxies. The uncertainty in $\mathcal{R}$ may not merely indicate the accuracy of our measurements but also reflects pointing errors. The average ratio is slightly lower than previous estimations of 11±3 (Aalto et al. 1991), 9.3±3.6 (Sage & Isbell 1991) and 11.3±3.3 for normal galaxies. Young & Sanders (1986) found no evidence for systematic variation in $\mathcal{R}$ with radius, and Sage & Isbell (1991) did not find clear evidence either. The average of all off-center points is somewhat less than the average of the centers. It has been suggested that galaxies which display variations in $\mathcal{R}$ have varying large-scale properties in their molecular cloud distributions. Thus, our lower estimation of the average ratio, $\mathcal{R}$, may not result merely from the

Table 3 Derived Parameters of ^{13}CO Detected Galaxies

Galaxy	τ_{13}	$N(\mathrm{H_2})$ (10^{21} cm^{-2})	$N(\mathrm{H_2})'$ (10^{21} cm^{-2})	log$L_{^{12}\mathrm{CO}}$ (K km s^{-1} pc^2)	log$L_{^{13}\mathrm{CO}}$ (K km s^{-1} pc^2)	T_{ex} (K)	X
(1)	(2)	(3)	(4)	(5)	(6)	(7)	(8)
M66	0.08	6.78 (0.13)	2.46(0.20)	$8.39^{+0.01}_{-0.01}$	$7.35^{+0.03}_{-0.04}$	52.88	0.72(0.06)
M108	0.12	3.59 (0.13)	1.75(0.32)	$8.39^{+0.02}_{-0.02}$	$7.49^{+0.07}_{-0.09}$	36.86	0.98(0.18)
NGC 3079	0.09	11.83 (0.19)	4.57(0.25)	$9.15^{+0.01}_{-0.01}$	$8.13^{+0.02}_{-0.02}$	49.37	0.77(0.04)
NGC 3184	0.09	1.30 (0.09)	0.44(0.20)	$7.87^{+0.03}_{-0.03}$	$6.85^{+0.16}_{-0.26}$	49.67	0.67(0.30)
NGC 3593	0.04	4.87 (0.16)	0.90(0.30)	$7.65^{+0.01}_{-0.01}$	$6.32^{+0.12}_{-0.18}$	107.17	0.37(0.12)
NGC 3628	0.08	14.53 (0.12)	5.40(0.54)	$8.72^{+0.00}_{-0.00}$	$7.68^{+0.04}_{-0.05}$	52.64	0.74(0.07)
NGC 3631	0.11	2.26 (0.10)	0.96(0.22)	$8.58^{+0.02}_{-0.02}$	$7.64^{+0.09}_{-0.11}$	40.28	0.85(0.20)
NGC 3672	0.26	3.12 (0.26)	3.16(0.29)	$8.93^{+0.04}_{-0.04}$	$8.34^{+0.04}_{-0.04}$	15.39	2.03(0.25)
NGC 3675	0.21	3.43 (0.21)	2.67(0.34)	$8.30^{+0.03}_{-0.03}$	$7.63^{+0.05}_{-0.06}$	19.51	1.56(0.22)
NGC 3810	0.12	2.48 (0.09)	1.18(0.23)	$8.32^{+0.02}_{-0.02}$	$7.42^{+0.08}_{-0.09}$	36.91	0.95(0.19)
NGC 3893	0.06	2.73 (0.11)	0.70(0.17)	$8.42^{+0.02}_{-0.02}$	$7.25^{+0.09}_{-0.12}$	72.17	0.52(0.13)
NGC 3938	0.12	1.49 (0.07)	0.69(0.19)	$8.07^{+0.02}_{-0.02}$	$7.17^{+0.10}_{-0.14}$	36.22	0.93(0.25)
NGC 4038	0.22	5.72 (0.40)	5.60(0.74)	$8.98^{+0.03}_{-0.03}$	$8.33^{+0.05}_{-0.06}$	18.23	1.96(0.29)
NGC 4039	0.12	7.99 (0.39)	4.14(0.64)	$9.13^{+0.02}_{-0.02}$	$8.22^{+0.06}_{-0.07}$	36.90	1.04(0.17)
NGC 4041	0.08	3.67 (0.13)	1.21(0.40)	$8.84^{+0.02}_{-0.02}$	$7.76^{+0.12}_{-0.17}$	56.94	0.66(0.22)
NGC 4088	0.11	4.38 (0.21)	2.03(0.40)	$8.45^{+0.02}_{-0.02}$	$7.52^{+0.08}_{-0.10}$	39.29	0.93(0.19)
NGC 4102	0.08	4.21 (0.14)	1.61(0.39)	$8.64^{+0.01}_{-0.01}$	$7.57^{+0.09}_{-0.12}$	55.60	0.77(0.19)
NGC 4157	0.11	3.58 (0.12)	1.59(0.36)	$8.36^{+0.01}_{-0.02}$	$7.44^{+0.09}_{-0.11}$	38.46	0.89(0.20)
NGC 4212	0.32	1.05 (0.31)	1.36(0.55)	$7.95^{+0.11}_{-0.15}$	$7.44^{+0.15}_{-0.23}$	11.77	2.58(1.30)
NGC 4254	0.13	5.11 (0.10)	2.78(0.21)	$8.63^{+0.01}_{-0.01}$	$7.78^{+0.03}_{-0.03}$	32.42	1.09(0.08)
NGC 4273	0.22	2.35 (0.16)	2.18(0.54)	$8.30^{+0.03}_{-0.03}$	$7.65^{+0.10}_{-0.12}$	18.24	1.85(0.48)
NGC 4298	0.19	2.54 (0.14)	1.74(0.24)	$8.33^{+0.02}_{-0.03}$	$7.61^{+0.06}_{-0.06}$	22.32	1.37(0.20)
NGC 4303	0.07	3.86 (0.10)	1.15(0.36)	$8.51^{+0.01}_{-0.01}$	$7.39^{+0.12}_{-0.16}$	64.15	0.60(0.19)
NGC 4312	0.57	1.19 (0.29)	2.60(0.59)	$8.07^{+0.10}_{-0.12}$	$7.75^{+0.09}_{-0.11}$	5.19	4.39(1.47)
NGC 4321	0.13	6.01 (0.16)	3.06(0.48)	$8.70^{+0.01}_{-0.01}$	$7.83^{+0.06}_{-0.07}$	34.16	1.02(0.16)
NGC 4402	0.19	3.16 (0.17)	2.33(0.31)	$8.43^{+0.02}_{-0.02}$	$7.72^{+0.05}_{-0.06}$	21.48	1.47(0.21)
NGC 4414	0.16	8.82 (0.18)	5.80(0.35)	$9.00^{+0.01}_{-0.01}$	$8.22^{+0.03}_{-0.03}$	26.52	1.32(0.08)
NGC 4419	0.24	5.36 (0.28)	5.51(0.63)	$8.65^{+0.02}_{-0.02}$	$8.04^{+0.05}_{-0.05}$	16.59	2.06(0.26)
NGC 4457	0.11	2.90 (0.12)	1.38(0.37)	$8.21^{+0.02}_{-0.02}$	$7.27^{+0.10}_{-0.14}$	39.79	0.95(0.26)
NGC 4501	0.25	5.93 (0.18)	5.62(0.50)	$8.70^{+0.01}_{-0.01}$	$8.09^{+0.04}_{-0.04}$	15.96	1.90(0.18)
NGC4527	0.21	7.44 (0.24)	6.50(0.57)	$8.80^{+0.01}_{-0.01}$	$8.11^{+0.04}_{-0.04}$	20.16	1.75(0.16)
NGC 4536	0.33	3.47 (0.23)	5.40(0.63)	$8.44^{+0.03}_{-0.03}$	$7.94^{+0.05}_{-0.05}$	11.62	3.11(0.42)
NGC 4568	0.19	4.89 (0.12)	3.76(0.59)	$8.61^{+0.01}_{-0.01}$	$7.91^{+0.06}_{-0.07}$	21.38	1.54(0.24)
NGC 4569	0.25	7.25 (0.24)	7.06(0.43)	$8.79^{+0.01}_{-0.01}$	$8.17^{+0.03}_{-0.03}$	16.27	1.95(0.13)
NGC 4631	0.21	2.35 (0.15)	2.13(0.40)	$7.70^{+0.03}_{-0.03}$	$7.02^{+0.07}_{-0.09}$	20.11	1.81(0.36)
NGC 4647	0.38	5.28 (0.37)	7.81(0.67)	$8.65^{+0.03}_{-0.03}$	$8.20^{+0.04}_{-0.04}$	9.47	2.96(0.33)
NGC 4654	0.13	3.36 (0.19)	1.77(0.57)	$8.45^{+0.02}_{-0.03}$	$7.60^{+0.12}_{-0.17}$	32.16	1.05(0.34)
NGC 4691	0.11	2.16 (0.12)	1.06(0.30)	$8.52^{+0.02}_{-0.02}$	$7.57^{+0.11}_{-0.15}$	42.02	0.98(0.29)
NGC 4736	0.36	4.86 (0.09)	8.03(0.41)	$7.61^{+0.01}_{-0.01}$	$7.14^{+0.02}_{-0.02}$	10.12	3.30(0.18)
NGC 4818	0.16	4.31 (0.28)	3.46(0.98)	$8.13^{+0.03}_{-0.03}$	$7.36^{+0.11}_{-0.14}$	26.41	1.61(0.47)
NGC 4826	0.19	9.63 (0.13)	7.72(0.30)	$7.52^{+0.01}_{-0.01}$	$6.81^{+0.02}_{-0.02}$	21.79	1.60(0.07)
NGC 4845	0.12	6.14 (0.30)	3.09(0.67)	$8.70^{+0.02}_{-0.02}$	$7.81^{+0.09}_{-0.11}$	35.55	1.01(0.22)

Column (1): Names of galaxies that had detections of ^{13}CO Column (2): The optical depth of ^{13}CO emission derived from Equation (5). Columns (3)–(4): The H_2 column density derived from ^{12}CO and ^{13}CO, respectively, from Equation (6) and Equation (8). Columns (5)–(6): ^{12}CO and ^{13}CO luminosities derived from Equation (9) and Equation (10) respectively. Column (7): Excitation temperature calculated by equating the H_2 column density derived both from ^{12}CO and ^{13}CO. Column (8): The X factor, calculated by dividing H_2 column density and CO integrated intensity, in the unit of 10^{20} cm^{-2}[K km s^{-1}]$^{-1}$.

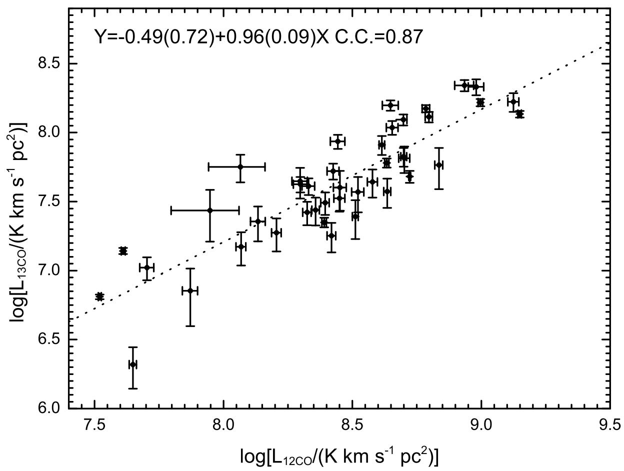

Fig. 2 The comparison between the ^{12}CO and ^{13}CO luminosity. A correlation is validated with a correlation coefficient (C.C.) of 0.87. The dotted line corresponds to the average ratio, $\mathcal{R}$.

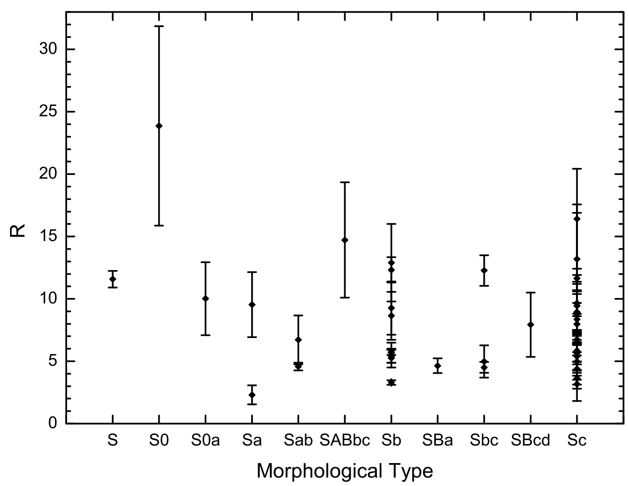

Fig. 3 The intensity ratio of ^{12}CO/^{13}CO, $\mathcal{R}$, is independent of the morphological type. There is no clear relationship between $\mathcal{R}$ and the morphological type evolution in subclasses of spirals.

different main beam efficiencies of different telescopes, but may also be due to the different samples of galaxies with regions larger than the center that are covered in a one-beam-sized field in our observations.

We compared ^{12}CO luminosity with ^{13}CO luminosity in Figure 2. Of course a tight correlation can be found because of the same distance and the deviation (which accounts for variations in $\mathcal{R}$). We could not determine why Taniguchi & Ohyama (1998) claimed that more luminous galaxies have lower ^{13}CO luminosity with respect to ^{12}CO. Perhaps a wider range of CO luminosity data of other galaxies is needed.

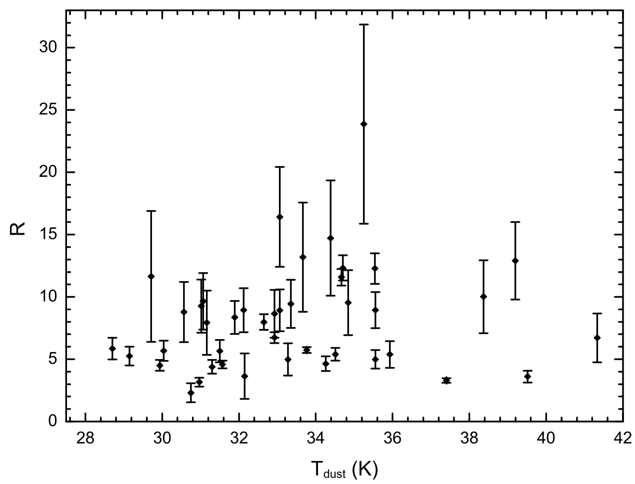

Fig. 4 The correlation between $\mathcal{R}$ and dust temperature. There seems to be little relationship between them below a temperature of 40 K.

Generally, it is suggested that the intensity ratio, $\mathcal{R}$, is a measure of the cloud environment in galaxies (Aalto et al. 1991; Aalto et al. 1995). High ratio values ($\mathcal{R}> 20$) might originate in turbulent, high-pressure gas in the centers of luminous interactive galaxies or mergers, intermediate values ($10 \leq\mathcal{R}\leq 15$) refer to normal starbursts, and low values ($\mathcal{R}\simeq 6$) represent the disk population of clouds. The deficiency of ^{13}CO due to isotope-selective photodissociation may alternatively account for a high $\mathcal{R}$.

Sage & Isbell (1991) found that the intensity ratio of ^{12}CO/^{13}CO $\mathcal{R}$ is independent of the morphological type. Our result in Figure 3 is similar to Young et al. (1989) and Sage & Solomon (1989): there is no clear relationship between the intensity ratio, $\mathcal{R}$, and the morphological type evolution in subclasses of spirals.

Figure 4 illustrates the relationship between $T_{\rm dust}$ and $\mathcal{R}$. It has been claimed that high CO luminosities in luminous far-infrared galaxies are due to a greater excitation temperature of CO gas rather than a higher mass quantity (Maloney & Black 1988; Stacey et al. 1991). However, we concluded the same results as Sage & Isbell (1991): there seems to be no clear relationship between them below a temperature of 40 K. Unfortunately, we were unable to test whether there exists a trend in $\mathcal{R}$ and $T_{\rm dust}$ beyond 40 K.

The CO-H$_2$ conversion factor gives us a direct way to estimate H$_2$ gas in molecular clouds through CO. In the Milky Way, we usually take a universal value of $X = 2 \times 10^{20}$ $\rm cm^{-2}$ $(\rm K\ km\ s^{-1})^{-1}$ as an estimation. For an estimation that is valid in other galaxies, we found an average value of $1.44 \pm 0.84 \times 10^{20}\,\rm cm^{-2}$ $(\rm K\ km\ s^{-1})^{-1}$, which is slightly lower than the standard value in the Milky Way.

5 SUMMARY

Using the PMO 13.7-m millimeter-wave telescope, we simultaneously observed the ^{12}CO, ^{13}CO and C^{18}O $J = 1 - 0$ rotational transitions in the centers of 58 nearby galaxies with relatively strong ^{12}CO emissions. We detected ^{13}CO emissions in 42 out of the 58 galaxies, but had a null detection of C^{18}O emission with a σ upper limit of 2 mK. The main two results are summarized as follows:

(1) We presented results of spectra, using the integrated intensity of both ^{12}CO and ^{13}CO emissions in each galaxy. Central beam ratios, $\mathcal{R}$, of ^{12}CO and ^{13}CO range mostly from 5 to 13, with an average value of 8.14±4.21, which is slightly lower than previous estimates for normal galaxies.

(2) We calculated ^{12}CO and ^{13}CO luminosities and clear correlations are validated. We computed the column density of H_2 gas from $I(^{13}\mathrm{CO})$ and then calibrated the X factor, finding an average value of $1.44 \pm 0.84 \times 10^{20}\ \mathrm{cm}^{-2}\ (\mathrm{K\ km\ s}^{-1})^{-1}$, which is slightly lower than the standard value in the Milky Way.

Acknowledgements We give special thanks to the staff of PMO Qinghai Station for their help.

References

Aalto, S., Booth, R. S., Black, J. H., & Johansson, L. E. B. 1995, A&A, 300, 369
Aalto, S., Johansson, L. E. B., Booth, R. S., & Black, J. H. 1991, A&A, 249, 323
Braine, J., Combes, F., Casoli, F., et al. 1993, A&AS, 97, 887
Daddi, E., Elbaz, D., Walter, F., et al. 2010, ApJ, 714, L118
Elfhag, T., Booth, R. S., Hoeglund, B., Johansson, L. E. B., & Sandqvist, A. 1996, A&AS, 115, 439
Gao, Y., & Solomon, P. M. 2004, ApJ, 606, 271
Helfer, T. T., Thornley, M. D., Regan, M. W., et al. 2003, ApJS, 145, 259
Leroy, A. K., Walter, F., Bigiel, F., et al. 2009, AJ, 137, 4670
Maloney, P., & Black, J. H. 1988, ApJ, 325, 389
Nishiyama, K., Nakai, N., & Kuno, N. 2001, PASJ, 53, 757
Paglione, T. A. D., Wall, W. F., Young, J. S., et al. 2001, ApJS, 135, 183
Rickard, L. J., Palmer, P., Morris, M., Zuckerman, B., & Turner, B. E. 1975, ApJ, 199, L75
Sage, L. J., & Isbell, D. W. 1991, A&A, 247, 320
Sage, L. J., & Solomon, P. M. 1989, ApJ, 342, L15
Sakamoto, K., Okumura, S. K., Ishizuki, S., & Scoville, N. Z. 1999, ApJS, 124, 403
Sanders, D. B., Mazzarella, J. M., Kim, D.-C., Surace, J. A., & Soifer, B. T. 2003, AJ, 126, 1607
Sanders, D. B., & Mirabel, I. F. 1996, ARA&A, 34, 749
Solomon, P. M., & de Zafra, R. 1975, ApJ, 199, L79
Solomon, P. M., Downes, D., Radford, S. J. E., & Barrett, J. W. 1997, ApJ, 478, 144
Solomon, P. M., & Sage, L. J. 1988, ApJ, 334, 613
Solomon, P. M., & Vanden Bout, P. A. 2005, ARA&A, 43, 677
Stacey, G. J., Geis, N., Genzel, R., et al. 1991, ApJ, 373, 423
Tan, Q.-H., Gao, Y., Zhang, Z.-Y., & Xia, X.-Y. 2011, RAA (Research in Astronomy and Astrophysics), 11, 787
Taniguchi, Y., & Ohyama, Y. 1998, ApJ, 507, L121
Wilson, T. L., Rohlfs, K., & Hüttemeister, S. 2009, Tools of Radio Astronomy (Springer-Verlag)
Young, J. S., & Sanders, D. B. 1986, ApJ, 302, 680
Young, J. S., & Scoville, N. Z. 1991, ARA&A, 29, 581
Young, J. S., Xie, S., Kenney, J. D. P., & Rice, W. L. 1989, ApJS, 70, 699
Young, J. S., Xie, S., Tacconi, L., et al. 1995, ApJS, 98, 219